Accurate simulation and thermal tuning by temperature-adaptive boundary interactions on quantum many-body systems

Ding-Zu Wang,[1] Guo-Feng Zhang,[1,*] Maciej Lewenstein,[2,3,†] and Shi-Ju Ran[4,‡]

[1]*School of Physics, Beihang University,100191,Beijing, China*
[2]*ICFO - Institut de Ciencies Fotoniques, The Barcelona Institute of Science and Technology, Av. Carl Friedrich Gauss 3, 08860 Castelldefels (Barcelona), Spain*
[3]*ICREA, Pg. Lluís Companys 23, 08010 Barcelona, Spain*
[4]*Department of Physics, Capital Normal University, Beijing 100048, China*

(Dated: May 3, 2021)

Constructing quantum Hamiltonians for simulating and controlling the exotic physics of many-body systems belongs to the most important topics of condensed matter physics and quantum technologies. The main challenge that hinders the future investigations is the extremely high complexity for either their numerical simulations or experimental realizations. In this work, we propose the temperature-adaptive entanglement simulator (TAES) that mimics and tunes the thermodynamics of the one-dimensional (1D) many-body system by embedding a small-size model in an entanglement bath. The entanglement bath is described by the interactions located at the boundaries of the small-size model, whose coupling constants are optimized by means of differentiable tensor network at target temperatures. With the benchmark on 1D spin chains, TAES surpasses the state-of-the-art accuracy compared with the existing finite-temperature approaches such as linearized and differential tensor renormalization group algorithms. By tuning the couplings of the entanglement bath with the temperature fixed, the bulk entropy exhibits similar behavior compared to that obtained by tuning the temperature. Our work provides novel opportunities of engineering the distribution of fluctuations and mimicking the non-equilibrium phenomena in a uniform temperature within the canonical ensemble framework using the optimized boundary interactions.

I. INTRODUCTION

The strong correlations may give rise to exotic phenomena in quantum many-body systems [1]. However, such systems suffer from high complexity, making their simulations in general challenging both numerically and experimentally. In the last two decades, numerical algorithms have achieved great success, including Monte Carlo approaches [2, 3], density matrix renormalization group [4, 5] and its variants [6–13], and tensor network (TN) methods [14–16]. Despite many inspiring progresses in the quantum many-body physics, such as topological spin liquids [17–19], there still exists a huge gap between the theoretical predictions and their experimental observations and applications. One reason is that natural materials with strong correlations are rare. Therefore, the methods to theoretically construct the Hamiltonians realizable on the artificial platforms, such as ultra-cold atoms [20] photonic systems [21, 22] and superconducting circuits [23], for the purposes of simulation [24] and control [25] are strongly desired.

The existing works suggested several ways of engineering effective Hamiltonians by, e.g., perturbation theory [26, 27] and magic angle spinning [28]. It was proposed to design the simulator Hamiltonians with two-spin interactions to simulate the ground-state energy of the Hamiltonians with multi-spin interactions [29]. TN also provides numerous possibilities in this respect. The density matrix renormalization group [4, 5] defines the effective Hamiltonians for the ground-state simulations of 1D quantum systems by optimizing the renormalization group transformations in the form of matrix product state [30]. A similar idea was proposed for simulating the time evolutions [31]. For the quantum lattice models in higher dimensions, the tree TN approximation was proposed and improved to obtain the effective Hamiltonians for simulating the ground states [32, 33] and thermodynamics [34–40].

In this work, we propose a method to construct the effective Hamiltonians, dubbed as temperature-adaptive entanglement simulator (TAES). It permits accurate simulations of finite-temperature properties of 1D quantum systems in the thermodynamic limit with small-size simulators. The accuracy of TAES surpasses the state-of-the-art thermodynamic methods including linearized and differentiable tensor renormalization group algorithms [41, 42]. On the boundaries of the TAES, the interactions are optimized for the targeted temperature (dubbed as bath temperature) to mimic the entanglement between the bulk and the infinite environment. With just small sizes, the bulk properties of the TAES optimally give those of the infinite-size system.

Subsequently, we treat the bath temperature as a tuning parameter to explore the controlling effects of the TAES. Our results indicate that the boundary interactions could play a similar role as the heat bath to affect the bulk properties, while the physical temperature remains uniform for the whole TAES. That implies the possibility of mimicking the properties of grand canonical ensembles in effective canonical ensembles. Furthermore, the entropic properties show that by lowering the bath temperature, the strength of fluctuations in the bulk is suppressed in a more drastic way than lowering the physical temperature. For the systems with topological degeneracy of the ground state [43, 44], an entropic deep is observed, which is a typical tuning effect from the entanglement bath.

* gf1978zhang@buaa.edu.cn
† maciej.lewenstein@icfo.eu
‡ sjran@cnu.edu.cn

II. TEMPERATURE-ADAPTIVE ENTANGLEMENT SIMULATION

A. *General considerations*

Consider an infinite-size 1D Hamiltonian $\hat{H} = \sum_n \hat{h}_{n,n+1}$. Its thermodynamic properties in a finite-size bulk can be obtained from the reduced density matrix (RDM)

$$\hat{\rho}^{\text{bulk}}(T) = \frac{1}{Z}\text{Tr}_{/\text{bulk}} e^{-\frac{\hat{H}}{T}}, \tag{1}$$

with T the temperature, Z the partition function, and $\text{Tr}_{/\text{bulk}}$ tracing over all degrees of freedom except those of the bulk. However, to calculate the finite-temperature density matrix of an infinite-size system $e^{-\frac{\hat{H}}{T}}$ is very challenging.

An efficient way to access the thermodynamics of infinite-size many-body system is to construct a finite-size effective model embedded in an "entanglement bath", which is known as quantum entanglement simulator (QES) [40]. The RDM of the QES by tracing over the bath degrees of freedom should optimally mimic the RDM of the infinite-size system. A QES is made of N sites in the bulk and two sites at the boundary. The Hamiltonian of a QES can be written as

$$\hat{H}^{\text{QES}} = \hat{\mathcal{H}}^L + \hat{H}^{\text{bulk}} + \hat{\mathcal{H}}^R. \tag{2}$$

The bulk Hamiltonian $\hat{H}^{\text{bulk}} = \sum_{n=1}^{N-1} \hat{h}_{n,n+1}$ contains the interactions of the N sites within the bulk, where $\hat{h}_{n,n+1}$ is the same as the local term of the infinite-size model. $\hat{\mathcal{H}}^L$ ($\hat{\mathcal{H}}^R$) is the interaction between the left (right) bath site and the physical spin at the left (right) end of the bulk. The dimension of the bath sites (denoted by χ) is flexible. It plays the same role as the virtual dimension cut-off in density matrix renormalization group (DMRG) [4, 5], and determines the upper bounds of the entanglement entropy that can be mimicked between the bulk of the infinite halves.

In this work, we aim to solve the following optimization problem

$$\min_{\hat{\mathcal{H}}^L, \hat{\mathcal{H}}^R} \|\hat{\rho}^{\text{bulk}}(T) - \hat{\rho}^{\text{QES}}(T)\| \tag{3}$$

with $\hat{\rho}^{\text{QES}}(T) = \text{Tr}_{\text{bath}} e^{-\frac{\hat{H}^{\text{QES}}}{T}}$ and Tr_{bath} tracing over all degrees of freedom of the bath sites. The boundary Hamiltonians $\hat{\mathcal{H}}^L$ and $\hat{\mathcal{H}}^R$ can be chosen as the renormalized Hamiltonians that optimally represents the couplings between the bulk and the infinite halves of the system. In the previous works of quantum entanglement simulation, the renormalization-group (RG) transformations can be given in the form of tensor network (TN), e.g., matrix product state (MPS) and tree projected entangled pair state [40]. Subsequently they can be optimized in a similar way as DMRG or its variant on trees. Since in DMRG, the RG transformations are optimized based on the ground state, the optimization problem actually becomes

$$\min_{\hat{\mathcal{H}}^L, \hat{\mathcal{H}}^R} \|\text{Tr}_{/\text{bulk}} |\psi_g\rangle\langle\psi_g| - \hat{\rho}^{\text{QES}}(T)\|, \tag{4}$$

with $|\psi_g\rangle$ the ground state of $\hat{H}$. Since the above bath optimization is to mimic the RDM of the ground state (zero temperature), we denote the corresponding RDM and the boundary Hamiltonians as

$$\hat{\rho}^{\text{QES}}(T|\tilde{T}^L = 0, \tilde{T}^R = 0) = \exp\left[-\frac{\hat{\mathcal{H}}^L(\tilde{T}=0) + \hat{H}^{\text{bulk}} + \hat{\mathcal{H}}^R(\tilde{T}=0)}{T}\right], \tag{5}$$

where we call $\tilde{T}^L$ and $\tilde{T}^R$ as the *bath temperatures*. The QES with $\hat{H}^{\text{QES}}(T|\tilde{T}^L = 0, \tilde{T}^R = 0)$ shows excellent accuracy to give the ground-state and low-temperature properties of the infinite system.

Here, we propose a TN approach to optimize the boundary Hamiltonians of the QES by directly solving Eq. (3), which we dub as *temperature-adaptive entanglement simulator* (TAES). In other words, the aim of TAES is to mimic $\hat{\rho}^{\text{bulk}}(T)$ instead of $\text{Tr}_{/\text{bulk}}|\psi_g\rangle\langle\psi_g|$, meaning to set the bath temperatures as $\tilde{T}^L = \tilde{T}^R = T$. The optimization algorithm is explained in detail in the Appendix.

B. *Benchmark on quantum Ising chain*

The benchmark data are demonstrated in Fig. 1 on the quantum Ising chain $\hat{H} = \sum_n \hat{S}^x_n \hat{S}^x_{n+1} - h\sum_m \hat{S}^z_m$. The relative errors of the free energy per site is defined as

$$\delta f = \frac{|f - f_{\text{exact}}|}{|f_{\text{exact}}|}, \tag{6}$$

with f_{exact} the analytic solution [45] and $\beta = 1/T$ the inverse temperature. We take the critical field $h = 0.5$, bulk size $N = 2$, and the virtual dimension cut-off (meaning the bath dimension in QES and TAES) as $\chi = 2$ and 20 as examples. TAES surpasses the state-of-the-art algorithms including the linearized and differentiable tensor renormalization group (LTRG and dTRG) algorithms.

Comparing with QES (taking $\tilde{T}^L = \tilde{T}^R = 0$), it is expected that its accuracy will eventually converge to that of TAES for the sufficiently low temperatures T. The accuracy of TAES is much higher than QES at the intermediate temperatures since it renormalizes the infinite halves of the system more properly by considering the "correct" bath temperatures, while optimizing the boundary Hamiltonians.

For $\chi = 2$ particularly, the bath sites can be equivalently treated as spin-1/2's [46]. In this case, the boundary Hamiltonians in the TAES of quantum Ising chain possess the following form

$$\hat{\mathcal{H}}^L = \sum_{\alpha=x,z} [J^L_{\alpha x} \hat{S}^\alpha_L \hat{S}^x_1 - \frac{1}{2} h_\alpha \hat{S}^\alpha_L], \tag{7}$$

$$\hat{\mathcal{H}}^R = \sum_{\alpha=x,z} [J^R_{x\alpha} \hat{S}^x_N \hat{S}^\alpha_R - \frac{1}{2} h_\alpha \hat{S}^\alpha_R]. \tag{8}$$

Taking $\tilde{T}^L = \tilde{T}^R = \tilde{T}$, the parameters in the boundary Hamiltonians versus $\tilde{T}$ are given in Fig. 2. Due to the symmetries of the system, we have

$$-J^L_{xz} = -J^R_{zx} \doteq J_{xz}, \quad h^L_x = h^R_x \doteq h_x, \tag{9}$$

$$J^L_{xx} = -J^R_{xx} \doteq J_{xx}, \quad h^L_z = h^R_z \doteq h_z. \tag{10}$$

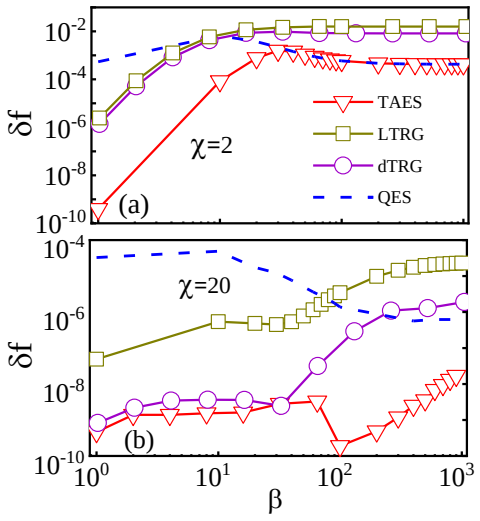

FIG. 1. (Color online) The relative errors of the free energy δf [Eq. (6)] versus β obtained by linearized/differentiable tensor renormalization group algorithms (in short LTRG [41] and dTRG [42], respectively), QES [40], and TAES.

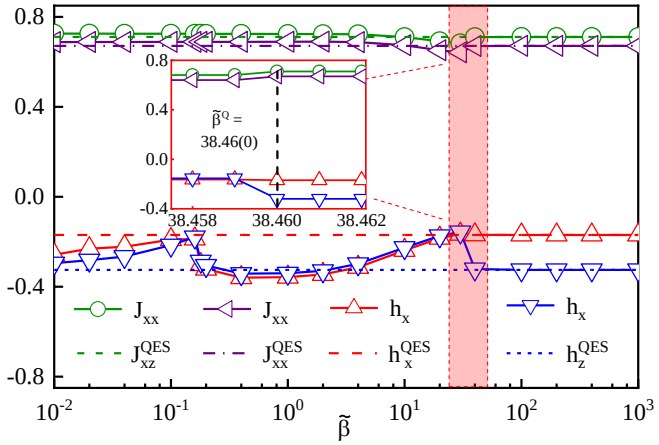

FIG. 2. (Color online) The coefficients of the boundary Hamiltonians versus the inverse bath temperatures $\tilde{\beta} = 1/\tilde{T}$. The dash lines give the coefficients at zero bath temperature [46]. The inset shows the zoom near the boundary-induced thermal quench point $\tilde{\beta}^Q$.

A discontinuous point is observed at $\tilde{\beta} = 1/\tilde{T} \simeq 38.46(0)$, which we dub as *boundary quench point* (BQP) $\tilde{\beta}^Q$. BQP indicates the bath temperature, below which the parameters in the boundary Hamiltonians of TAES becomes approximately identical to those of the QES. Consistently, the error for $\tilde{\beta} > \tilde{\beta}^Q$ is small, as shown in Fig. 1 (a). Note we take $\tilde{\beta} = \beta$ in the TAES.

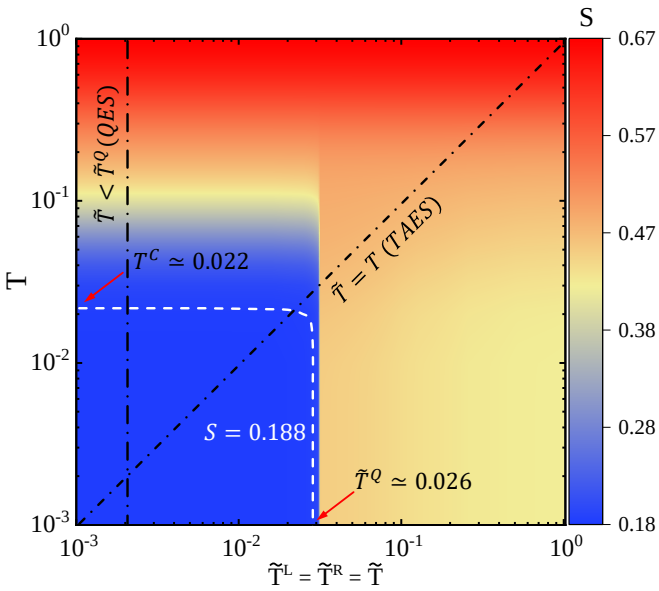

FIG. 3. (Color online) The average bulk entropy S of the TAES for the quantum Ising model at different temperatures T and bath temperatures $\tilde{T}^L = \tilde{T}^R = \tilde{T}$. We take the transverse field at the critical point $h_x = 0.5$. S is suppressed to $S = 0.188$ for about $T < 0.022$ and $\tilde{T} < 0.026$.

III. THERMAL TUNING BY TEMPERATURE-ADAPTIVE BOUNDARY HAMILTONIANS

A. *General considerations*

The superior accuracy of TAES implies that $\hat{\mathcal{H}}^L(\tilde{T})$ and $\hat{\mathcal{H}}^R(\tilde{T})$ can accurately represent the infinite halves of the system at the temperature $T = \tilde{T}$. It is then a natural question whether $\tilde{T}$ could play a similar role as the physical temperature T to tune the fluctuations of the bulk.

To proceed, we consider the density matrix of the TAES at the temperature T

$$\hat{\rho}^{\text{TAES}}(T|\tilde{T}^L, \tilde{T}^R) = \frac{1}{Z} e^{\left[-\frac{\hat{\mathcal{H}}^L(\tilde{T}^L) + \hat{H}^{\text{bulk}} + \hat{\mathcal{H}}^R(\tilde{T}^R)}{T}\right]}, \quad (11)$$

with Z the partition function. The fluctuations of the spins in the bulk are characterized by the on-site entropy

$$S_n = -\text{Tr}(\hat{\rho}_n \ln \hat{\rho}_n), \quad (12)$$

with $\hat{\rho}_n = \text{Tr}_{/n}\hat{\rho}^{\text{TAES}}(T|\tilde{T}^L, \tilde{T}^R)$ the RDM of the n-th spin in the bulk.

Fig. 3 demonstrates the average bulk entropy $S = \sum_{n=1}^{N} S_n/N$ with different T and $\tilde{T}(= \tilde{T}^L = \tilde{T}^R)$ with the bulk size $N = 8$. We shall stress that even for $\tilde{T} \neq T$, the "physical" temperature of whole TAES is uniformly T, according to Eq. (11). The bath temperature $\tilde{T}$ only determines the values of the coefficients in the boundary Hamiltonians (see Fig. 2).

When $\tilde{T}$ and T are both low, the bulk entropy S is suppressed to a low value with $S < 0.19$ approximately (see the

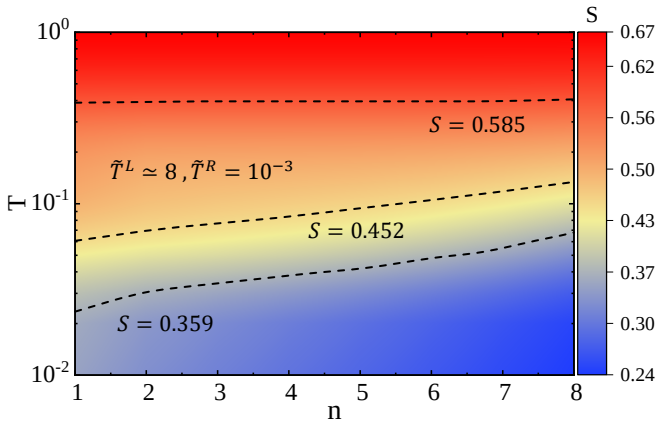

FIG. 4. (Color online) The on-site entropy S_n of the TAES for the quantum Ising model on different site n of the bulk at different temperatures T. Taking the left and right bath temperatures as $\tilde{T}^L \simeq 8$ and $\tilde{T}^R \simeq 10^{-3}$, respectively, a slope of the spatial distribution of the fluctuations is observed.

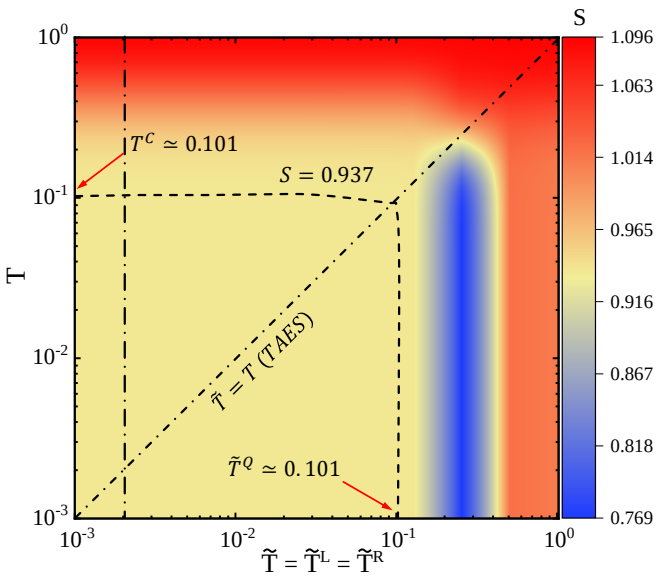

FIG. 5. (Color online) The average on-site entropy S of the TAES for the spin-1 Heisenberg model at different temperatures T and bath temperatures $\tilde{T}$. A entropy deep is observed near $\tilde{T} = 0.25$ for approximately $T < 0.98$.

blue area). By lowering $\tilde{T}$ with fixed T, S drops to $S \simeq 0.188$ at $\tilde{T} \simeq \tilde{T}^Q$ in a much more drastic way, compared with the case by lowering T where S drops to $S \simeq 0.188$ at $T = T^C$ with fixed $\tilde{T}(< \tilde{T}^Q)$. Even $\tilde{T}$ and T stand for completely different meanings, we observe $\tilde{T}^Q \simeq T^C + O(10^{-3})$, which indicates certain equivalence in scaling between these two parameters. One reason from the perspective of quantum simulation could be the fact that the TAES gives the optimal effective model to mimic the infinite system and accurately predicts the crossover temperature, where one takes $T = \tilde{T}$.

B. *Benchmark on quantum Ising and spin-1 Heisenberg chains*

The entanglement bath in the TAES could affect the fluctuations in a similar manner as a source of heat. For $\tilde{T} < T$ as an example, the fluctuation of the spins close to the entanglement bath is slightly smaller than the spin in the middle of the bulk. In Fig. 4, we show the on-site entropy S_n at different sites by taking different bath temperatures with $\tilde{T}^L \simeq 8$ and $\tilde{T}^R \simeq 10^{-3}$. The physical temperature is still uniformly T and the system is still described by the Boltzmann distribution as Eq. (11). The spatial distribution of S_n shows non-zero gradient in the bulk of the TAES. It indicates that the entanglement bath with a low (high) $\tilde{T}$ tends to drive the system into an ordered (disordered) state, similar to a heat bath with a low (high) physical temperature. It is interesting to note that a system should be in generally described by a grand canonical ensemble [47], while we only use the canonical ensemble.

For the many-body systems that possess non-trivial topological properties, the entanglement bath can also affect the fluctuations by tuning the bath temperatures. We take the spin-1 Heisenberg chain [48] as an example, where the Hamiltonian reads $\hat{H} = \sum_n (\hat{S}_n^x \hat{S}_{n+1}^x + \hat{S}_n^y \hat{S}_{n+1}^y + \hat{S}_n^z \hat{S}_{n+1}^z)$ with $\hat{S}_n^\alpha$ ($\alpha = x, y, z$) the spin-1 operator on the n-th site.

Fig. 5 demonstrates $S = \sum_{n=1}^N S_n/N$ with different T and $\tilde{T}(= \tilde{T}^L = \tilde{T}^R)$ with the bulk size $N = 4$. When T and $\tilde{T}$ are both low, the bulk entropy is suppressed $S < 0.937$ and eventually converges to that of the ground state. The low-temperature S of the spin-1 model is much higher than that of the spin-$1/2$ model possibly due to its two-fold topological degeneracy of the ground state. We have $T^C \simeq \tilde{T}^Q \simeq 0.101$.

With T fixed, we find that S does not monotonously decrease with $\tilde{T}$. A deep of S (see the blue region) appears before the system enters the low-entropy region. It means the quantum fluctuations from the degenerate ground states and the thermal fluctuations are simultaneously suppressed. Such an entropy deep is a typical thermal effects from tuning the entanglement bath, since the QES (with $\tilde{T} = const. < \tilde{T}^Q$) and TAES (with $\tilde{T} = T$) lines do not pass through the deep. It means that the entropy deep will not be observed in the infinite-size system but in its simulators (QES and TAES). The deep would appear when taking $\tilde{T} = kT$ for $k > 1$.

IV. METHOD

Let us start with the Hamiltonian of 1D quantum many-body model given by

$$\hat{H} = \sum_{n=1}^{N} \hat{h}_{n,n+1}, \tag{13}$$

where we take the number of sites $N \to \infty$. The partition function can be represented by $e^{-\tau \hat{H}}$ as

$$Z = \mathrm{Tr}(e^{-\beta \hat{H}}) = \mathrm{Tr}[(e^{-\tau \hat{H}})^K], \tag{14}$$

with the Trotter slice $\tau \to 0$ and the inverse temperature $\beta = 1/T = \tau K$. In each slice, we use the second-order Trotter-

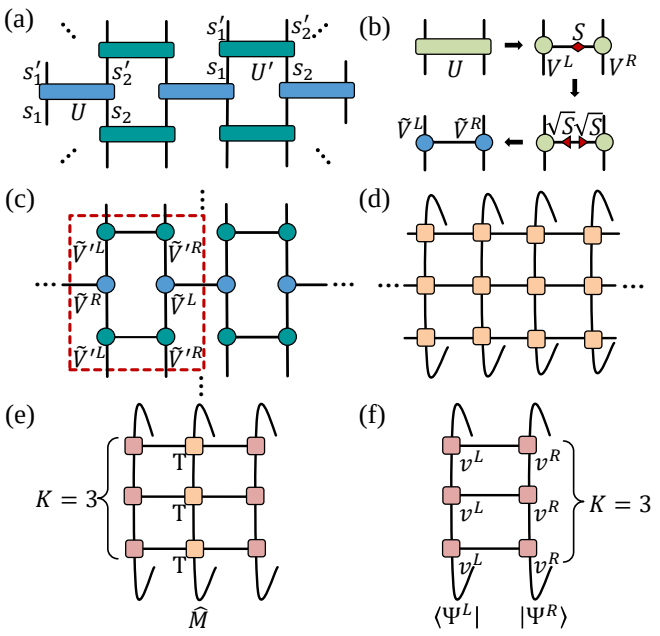

FIG. 6. (Color online) (a) Tensor network representation of the density matrix $e^{-\beta\hat{H}}$ formed by U in Eq. (16). (b) Decompose U to get $\tilde{V}^L$ and $\tilde{V}^R$. (c) The brick-wall TN. (d) Contract local tensors to obtain the square TN. (e) The illustration of $\langle\Psi^L|\hat{M}|\Psi^R\rangle$. (f) The illustration of $\langle\Psi^L|\Psi^R\rangle$. In this figure, we take $K = 3$ as an example.

Suzuki decomposition

$$e^{-\tau\hat{H}} \simeq e^{-\frac{\tau}{2}\sum_{\text{odd }n}\hat{h}_{n,n+1}} e^{-\tau\sum_{\text{even }n}\hat{h}_{n,n+1}} e^{-\frac{\tau}{2}\sum_{\text{odd }n}\hat{h}_{n,n+1}}. \tag{15}$$

Then Z can be represented as a TN [Fig. 6 (a)] formed by the fourth-order tensors

$$U_{s_1s_2,s_1's_2'} = \langle s_1s_2|e^{-\tau\hat{h}_{n,n+1}}|s_1's_2'\rangle, \tag{16}$$

$$U'_{s_1s_2,s_1's_2'} = \langle s_1s_2|e^{-\frac{\tau}{2}\hat{h}_{n,n+1}}|s_1's_2'\rangle. \tag{17}$$

The partition function can be obtained by contracting all the bonds in the TN. Decompose U by singular-value decomposition as

$$U_{s_1s_2,s_1's_2'} = \sum_\alpha V^L_{s_1s_1',\alpha} S_\alpha V^R_{s_2s_2',\alpha}, \tag{18}$$

where the diagonal matrix S contains the singular values. For convenience, we introduce $\tilde{V}^L = V^L\sqrt{S}$ and $\tilde{V}^R = V^R\sqrt{S}$ [Fig. 6 (b)]. The tensors $\tilde{V}'^L$ and $\tilde{V}'^R$ are obtained in a similar way by decomposing U'. Then we obtain a brick-wall TN [Fig. 6 (c)].

Implementing the contraction of $\tilde{V}^L$, $\tilde{V}^R$, $\tilde{V}'^L$, and $\tilde{V}'^R$ as illustrated in Fig. 6 (c), we have a square TN formed by one inequivalent tensor. It is infinite along the spatial (parallel) direction, and has K layers along the imaginary-time (vertical) direction with periodic boundary condition. Fig. 6 (d) illustrate the TN taking $K = 3$ as an example.

Similar to the transfer-matrix renormalization group algorithm [8], such a TN can be contracted by solving the left and right dominant eigenstates ($|\Psi^L\rangle$ and $|\Psi^R\rangle$) of the transfer

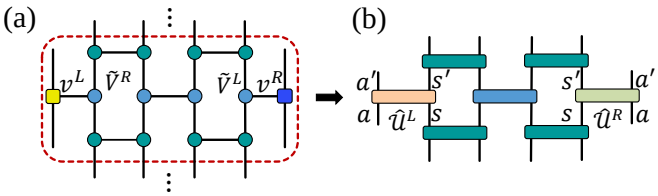

FIG. 7. (Color online) (a) Tensor network representation of the density matrix with the optimized v^L and v^R. (b) The imaginary-time evolution operator $e^{-\tau\hat{H}}$.

operator $\hat{M}$ that is formed by an infinite column of the tensors. With the translational invariance, we assume that $|\Psi^L\rangle$ and $|\Psi^R\rangle$ are in the form of uniform MPS [49] with periodic boundary condition, formed by the inequivalent tensors v^L and v^R, respectively. The dominant eigenvalue can be calculated by maximizing

$$\lambda = \max_{v^L,v^R} \frac{\langle\Psi^L|\hat{M}|\Psi^R\rangle}{\langle\Psi^L|\Psi^R\rangle}, \tag{19}$$

where the numerator and denominator are illustrated in Fig. 6 (e) and (f), respectively. We have $Z = \lambda^N$. The free energy per site $f = -\frac{1}{\beta}\ln\lambda$ satisfies

$$f = \max_{v^L,v^R}\left[-\frac{1}{\beta}\Big(\ln\langle\Psi^L|\hat{M}|\Psi^R\rangle - \ln\langle\Psi^L|\Psi^R\rangle\Big)\right]. \tag{20}$$

To solve the maximization problem, we iteratively update v^L and v^R as

$$v^L \leftarrow v^L + \eta\frac{\partial f}{\partial v^L}, \tag{21}$$

$$v^R \leftarrow v^R + \eta\frac{\partial f}{\partial v^R}, \tag{22}$$

where η is a small positive number known as the gradient step. The gradients $\frac{\partial f}{\partial v^{L(R)}}$ are calculated by the auto-differential technique of Pytorch [50, 52].

For the given inverse temperature β, the v^L and v^R that maximize f give the imaginary-time evolution operator of the bath Hamiltonians (Fig. 7) as

$$\hat{\mathcal{U}}^L_{aa',ss'} = \sum_\alpha v^L_{aa',\alpha}\tilde{V}^R_{ss',\alpha}, \tag{23}$$

$$\hat{\mathcal{U}}^R_{ss',aa'} = \sum_\alpha \tilde{V}^L_{ss',\alpha} v^R_{aa'\alpha}. \tag{24}$$

with a and a' the virtual bonds of the uMPS's. $\hat{\mathcal{U}}^L$ and $\hat{\mathcal{U}}^R$ can be regarded as the coefficients of local operators as $\hat{\mathcal{U}}^{L(R)} = \sum_{asa's'}\hat{\mathcal{U}}^{L(R)}_{aa',ss'}|as\rangle\langle a's'|$.

As shown in Fig. 7 (b), the evolution operator in an imaginary-time slice is approximated as

$$e^{-\tau\hat{H}} \simeq \hat{\mathcal{U}}^L e^{-\tau\sum_{n=1}^N\hat{h}_{n,n+1}}\hat{\mathcal{U}}^R, \tag{25}$$

with N the number of spins inside the finite-size bulk. The bath Hamiltonians are obtained as

$$\hat{\mathcal{H}}^{L(R)} = -\frac{\ln\hat{\mathcal{U}}^{L(R)}}{\tau}. \tag{26}$$

The Hamiltonian $\hat{H}^{\text{TAES}}$ for the simulator is the sum of $\hat{h}_{n,n+1}$ with $\hat{\mathcal{H}}^L$ and $\hat{\mathcal{H}}^R$ on its boundary

$$\hat{H}^{\text{TAES}} = \hat{\mathcal{H}}^L + \sum_{n=1}^{N} \hat{h}_{n,n+1} + \hat{\mathcal{H}}^R \tag{27}$$

For $\dim(a) = \dim(a') = 2$ particularly, $\{|a\rangle\}$ can be defined as the basis of spin-$1/2$. The bath Hamiltonians can be expanded as the summation of spin operators

$$\hat{\mathcal{H}}^{L(R)} = \sum_{\mu,\mu'=0,x,y,z} J^{L(R)}_{\mu\mu'} \hat{S}^{\mu} \otimes \hat{S}^{\mu'}, \tag{28}$$

where $\hat{S}^0$ represents an identity, $J^{L(R)}_{\mu 0}$ and $J^{L(R)}_{0\mu'}$ give the magnetic fields.

V. SUMMARY AND PERSPECTIVE

In summary, we propose the temperature-adaptive quantum simulation to accurately obtain the finite-temperature properties of 1D quantum many-body systems in the thermodynamic limit. Our idea is to construct a small-size simulator embedded in an entanglement bath, whose physical properties in the bulk optimally give those of the targeted infinite-size models. The interactions for the entanglement bath are optimized to adapt the temperature. With the benchmark on the 1D spin chains, TAES surpasses the state-of-the-art accuracy compared with the existing finite-temperature approaches.

Moreover, the entanglement bath can also be used to thermodynamically control the physical properties of the systems. The bath temperature $\tilde{T}$, to which the entanglement bath is adapted in the optimization process, could play a similar role as the physical temperature T to alter the fluctuations of the bulk. The entanglement bath could affect the bulk in a similar manner as the heat bath, while the whole system is described by the canonical ensemble. In specific, we observe that lowering $\tilde{T}$ could suppress the entropy in a more drastic way than lowering $\tilde{T}$. For the spin-1 chain whose ground state possesses topological degeneracy, a entropic "deep" is observed by tuning the bath temperature, where both thermal and quantum fluctuations are suppressed.

TAES can be readily generalized to the simulation and tuning on higher-dimensional quantum lattice models [33, 40]. Our work could shed light on designing experimental-friendly Hamiltonians and studying quantum thermodynamics, such as quantum thermal engines and quantum batteries [51], with the presence of strong correlations.

ACKNOWLEDGMENT

The authors are grateful to Gang Su, Wei Li, Han Li, Kai Xu, Han-Jie Zhu and Bin-Bin Chen for stimulating discussions. This work is supported by NSFC (No. 12004266, No. 11834014 and Grant No. 12074027), Beijing Natural Science Foundation (Grant No. 1192005 and No. Z180013), Foundation of Beijing Education Committees (No. KM202010028013), and the Academy for Multidisciplinary Studies, Capital Normal University. ICFO group acknowledges support from ERC AdG NOQIA, Agencia Estatal de Investigación ("Severo Ochoa" Center of Excellence CEX2019-000910-S, Plan National FIDEUA PID2019-106901GB-I00/10.13039 / 501100011033, FPI), Fundació Privada Cellex, Fundació Mir-Puig, and from Generalitat de Catalunya (AGAUR Grant No. 2017 SGR 1341, CERCA program, QuantumCAT -U16-011424 , co-funded by ERDF Operational Program of Catalonia 2014-2020), MINECO-EU QUANTERA MAQS (funded by State Research Agency (AEI) PCI2019-111828-2 / 10.13039/501100011033), EU Horizon 2020 FET-OPEN OPTOLogic (Grant No 899794), and the National Science Centre, Poland-Symfonia Grant No. 2016/20/W/ST4/00314, Marie Sklodowska-Curie grant STRETCH No 101029393.

[1] P. Coleman, *Introduction to Many-Body Physics* (Cambridge University Press, Cambridge, England, 2015).
[2] C. Jacoboni and L. Reggiani, The monte carlo method for the solution of charge transport in semiconductors with applications to covalent materials, Rev. Mod. Phys. **55**, 645 (1983).
[3] W. M. C. Foulkes, L. Mitas, R. J. Needs, and G. Rajagopal, Quantum Monte Carlo simulations of solids, Rev. Mod. Phys. **73**, 33 (2001).
[4] S. R. White, Density matrix formulation for quantum renormalization groups, Phys. Rev. Lett. **69**, 2863 (1992).
[5] S. R. White, Density-matrix algorithms for quantum renormalization groups, Phys. Rev. B **48**, 10345 (1993).
[6] R. J. Bursill, T. Xiang, and G. A. Gehring, The density matrix renormalization group for a quantum spin chain at nonzero temperature, Journal of Physics Condensed Matter **8**, L583 (1996).
[7] S. Moukouri and L. G. Caron, Thermodynamic Density Matrix Renormalization Group Study of the Magnetic Susceptibility of Half-Integer Quantum Spin Chains, Phys. Rev. Lett. **77**, 4640 (1996).
[8] X. Wang and T. Xiang, Transfer-matrix density-matrix renormalization-group theory for thermodynamics of one-dimensional quantum systems, Phys. Rev. B **56**, 5061 (1997).
[9] N. Shibata, Thermodynamics of the Anisotropic Heisenberg Chain Calculated by the Density Matrix Renormalization Group Method, Journal of the Physical Society of Japan **66**, 2221 (1997).
[10] K. A. Hallberg, Density-matrix algorithm for the calculation of dynamical properties of low-dimensional systems, Phys. Rev. B **52**, R9827 (1995).
[11] S. Ramasesha, S. K. Pati, H. Krishnamurthy, Z. Shuai, and J. Brédas, Low-lying electronic excitations and nonlinear optic properties of polymers via symmetrized density matrix renormalization group method, Synthetic Metals **85**, 1019 (1997).
[12] T. D. Kühner and S. R. White, Dynamical correlation functions using the density matrix renormalization group, Phys. Rev. B

60, 335 (1999).
[13] E. Jeckelmann, Dynamical density-matrix renormalization-group method, Phys. Rev. B **66**, 045114 (2002).
[14] S.-J. Ran, E. Tirrito, C. Peng, X. Chen, L. Tagliacozzo, G. Su, and M. Lewenstein, Tensor Network Contractions, Vol. 964 (Springer, Cham, Switzerland, 2020).
[15] R. Orús, A practical introduction to tensor networks: Matrix product states and projected entangled pair states, Annals of Physics **349**, 117 (2014).
[16] A. Weichselbaum, Non-abelian symmetries in tensor networks: A quantum symmetry space approach, Annals of Physics **327**, 2972 (2012).
[17] S. Yan, D. A. Huse, and S. R. White, Spin-Liquid Ground State of the S = 1/2 Kagome Heisenberg Antiferromagnet, Science **332**, 1173 (2011).
[18] Z. A. Kelly, M. J. Gallagher, and T. M. McQueen, Electron doping a kagome spin liquid, Phys. Rev. X **6**, 041007 (2016).
[19] B. Fåk, E. Kermarrec, L. Messio, B. Bernu, C. Lhuillier, F. Bert, P. Mendels, B. Koteswararao, F. Bouquet, J. Ollivier, A. D. Hillier, A. Amato, R. H. Colman, and A. S. Wills, Kapellasite: A kagome quantum spin liquid with competing interactions, Phys. Rev. Lett. **109**, 037208 (2012).
[20] M. Lewenstein, A. Sanpera, V. Ahufinger, B. Damski, A. Sen, and U. Sen, Ultracold atomic gases in optical lattices: mimicking condensed matter physics and beyond, Advances in Physics **56**, 243 (2007).
[21] D. Roy, C. M. Wilson, and O. Firstenberg, Colloquium: Strongly interacting photons in one-dimensional continuum, Rev. Mod. Phys. **89**, 021001 (2017).
[22] A. Peruzzo, M. Lobino, J. C. F. Matthews, N. Matsuda, A. Politi, K. Poulios, X.-Q. Zhou, Y. Lahini, N. Ismail, K. Wörhoff, Y. Bromberg, Y. Silberberg, M. G. Thompson, and J. L. OBrien, Quantum Walks of Correlated Photons, Science **329**, 1500 (2010).
[23] A. A. Houck, H. E. Türeci, and J. Koch, On-chip quantum simulation with superconducting circuits, Nature Physics **8**, 292 (2012).
[24] I. M. Georgescu, S. Ashhab, and F. Nori, Quantum simulation, Rev. Mod. Phys. **86**, 153 (2014).
[25] C. P. Koch, M. Lemeshko, and D. Sugny, Quantum control of molecular rotation, Rev. Mod. Phys. **91**, 035005 (2019).
[26] L.-M. Duan, E. Demler, and M. D. Lukin, Controlling spin exchange interactions of ultracold atoms in optical lattices, Phys. Rev. Lett. **91**, 090402 (2003).
[27] A. Micheli, G. K. Brennen, and P. Zoller, A toolbox for lattice-spin models with polar molecules, Nature Physics **2**, 341 (2006).
[28] A. Ajoy, U. Bissbort, D. Poletti, and P. Cappellaro, Selective decoupling and hamiltonian engineering in dipolar spin networks, Phys. Rev. Lett. **122**, 013205 (2019).
[29] S. Bravyi, D. P. DiVincenzo, D. Loss, and B. M. Terhal, Quantum simulation of many-body hamiltonians using perturbation theory with bounded-strength interactions, Phys. Rev. Lett. **101**, 070503 (2008).
[30] S. Östlund and S. Rommer, Thermodynamic limit of density matrix renormalization, Phys. Rev. Lett. **75**, 3537 (1995).
[31] H. N. Phien, G. Vidal, and I. P. McCulloch, Infinite boundary conditions for matrix product state calculations, Phys. Rev. B **86**, 245107 (2012).
[32] S.-J. Ran, Ab initio optimization principle for the ground states of translationally invariant strongly correlated quantum lattice models, Phys. Rev. E **93**, 053310 (2016).
[33] S.-J. Ran, A. Piga, C. Peng, G. Su, and M. Lewenstein, Few-body systems capture many-body physics: Tensor network approach, Phys. Rev. B **96**, 155120 (2017).
[34] S.-J. Ran, W. Li, B. Xi, Z. Zhang, and G. Su, Optimized decimation of tensor networks with super-orthogonalization for two-dimensional quantum lattice models, Phys. Rev. B **86**, 134429 (2012).
[35] P. Czarnik, L. Cincio, and J. Dziarmaga, Projected entangled pair states at finite temperature: Imaginary time evolution with ancillas, Phys. Rev. B **86**, 245101 (2012).
[36] S.-J. Ran, B. Xi, T. Liu, and G. Su, Theory of network contractor dynamics for exploring thermodynamic properties of two-dimensional quantum lattice models, Phys. Rev. B **88**, 064407 (2013).
[37] P. Czarnik and J. Dziarmaga, Variational approach to projected entangled pair states at finite temperature, Phys. Rev. B **92**, 035152 (2015).
[38] P. Corboz, P. Czarnik, G. Kapteijns, and L. Tagliacozzo, Finite correlation length scaling with infinite projected entangled-pair states, Phys. Rev. X **8**, 031031 (2018).
[39] P. Czarnik and P. Corboz, Finite correlation length scaling with infinite projected entangled pair states at finite temperature, Phys. Rev. B **99**, 245107 (2019).
[40] S.-J. Ran, B. Xi, C. Peng, G. Su, and M. Lewenstein, Efficient quantum simulation for thermodynamics of infinite-size many-body systems in arbitrary dimensions, Phys. Rev. B **99**, 205132 (2019).
[41] W. Li, S.-J. Ran, S.-S. Gong, Y. Zhao, B. Xi, F. Ye, and G. Su, Linearized tensor renormalization group algorithm for the calculation of thermodynamic properties of quantum lattice models, Phys. Rev. Lett. **106**, 127202 (2011).
[42] B.-B. Chen, Y. Gao, Y.-B. Guo, Y. Liu, H.-H. Zhao, H.-J. Liao, L. Wang, T. Xiang, W. Li, and Z. Y. Xie, Automatic differentiation for second renormalization of tensor networks, Phys. Rev. B **101**, 220409 (2020).
[43] N. Read and S. Sachdev, Valence-bond and spin-peierls ground states of low-dimensional quantum antiferromagnets, Phys. Rev. Lett. **62**, 1694 (1989).
[44] T. Lan, J. C. Wang, and X.-G. Wen, Gapped domain walls, gapped boundaries, and topological degeneracy, Phys. Rev. Lett. **114**, 076402 (2015).
[45] R. J. Baxter, Exactly Solved Models in Statistical Mechanics (Academic Press, 1982).
[46] S.-J. Ran, C. Peng, G. Su, and M. Lewenstein, Controlling the phase diagram of finite spin-$\frac{1}{2}$ chains by tuning the boundary interactions, Phys. Rev. B **98**, 085111 (2018).
[47] M. C. Mackey, The dynamic origin of increasing entropy, Rev. Mod. Phys. **61**, 981 (1989).
[48] S. R. White and D. A. Huse, Numerical renormalization-group study of low-lying eigenstates of the antiferromagnetic S=1 Heisenberg chain, Phys. Rev. B **48**, 3844 (1993).
[49] M. Fannes, B. Nachtergaele, and R. F. Werner, Finitely correlated states on quantum spin chains, Communications in Mathematical Physics **144**, 443 (1992).
[50] A. Paszke, G. Chanan, Z. Lin, S. Gross, E. Yang, L. Antiga, and Z. Devito, Automatic differentiation in PyTorch, *in Conference on Neural Information Processing Systems* (NIPS, Long Beach, CA, 2017).
[51] S. Julià-Farré, T. Salamon, A. Riera, M. N. Bera, and M. Lewenstein, Bounds on the capacity and power of quantum batteries, Phys. Rev. Research **2**, 023113 (2020) .
[52] The official website of PyTorch is at `https://pytorch.org/`